Nanomaterials

DOI: 10.1002/ange.201106004

Single-Layer Semiconducting Nanosheets: High-Yield Preparation and Device Fabrication**

*Zhiyuan Zeng, Zongyou Yin, Xiao Huang, Hai Li, Qiyuan He, Gang Lu, Freddy Boey, and Hua Zhang**

Two-dimensional (2D) nanomaterials have been receiving great attention in recent years because they show unusual physical properties which are the result of a quantum size effect associated to their ultra-thin structure.[1] As a typical example, graphene, a 2D single layer of carbon atoms of honeycomb lattice structure, has shown exceptional electronic, optical, thermal, and mechanical properties.[2]

Transition-metal dichalcogenides[3] (e.g. MoS_2, WS_2, TiS_2, TaS_2, and ZrS_2) and hexagonal boron nitride (h-BN)[4] have also been extensively studied and applied in catalysis,[3a] energy storage,[3b] and electronics.[3c,d] The common feature of these materials is that the bulk material forms are layered structures with strong covalent bonding in each layer and weak van der Waals forces between the layers. Therefore, single or few-layer nanosheets of these materials can be obtained by using adhesive tapes for mechanical cleavage.[5] However, this method is limited to the fabrication of a small amount of single-layer nanosheet materials with low reproducibility, which is disadvantageous for their application in electronic devices. Another useful method, which involves plasma etching and unzipping of nanotubes, has been employed to produce single-layer graphene[6] and BN[7] nanosheets (or ribbons). Unfortunately, such procedure is not feasible for solution-phase fabrication of large amounts. Therefore, a procedure including solution-phase exfoliation and direct growth of single or few-layer 2D materials has been developed.[3b,8]

Direct dispersion and ultrasonication of layered materials in common solvents, such as *N*-methylpyrrolidone (NMP) and dimethylformamide (DMF), have been used to prepare graphene[9] and few-layer h-BN sheets.[10] Recently, this method was employed to fabricate mono- and few-layer nanosheets from a series of layered compounds including MoS_2, WS_2, $MoSe_2$, $MoTe_2$, $TaSe_2$, $NbSe_2$, $NiTe_2$, BN, and Bi_2Te_3.[11] However, the direct dispersion and ultrasonication method, which simply relies on the solvent to minimize the energy of exfoliation, faces difficulties in the high-yield production of single-layer nanosheets.

Alternatively, graphite, h-BN, and transition-metal dichalcogenides can be intercalated by using various kinds of intercalates, such as organic molecules, alkali metals and transition-metal halides.[12] Exfoliation of the intercalated compounds by ultrasonication can give rise to single- and few-layer 2D nanosheets.[8a] However, except for graphene, a facile and reliable method for high-yield production of high-quality, single-layer nanosheets of the aforementioned materials has not been developed so far. Taking MoS_2 and WS_2 as examples, the preparation of single-layer materials can be realized by using *n*-butyl lithium in hexane as the intercalation agent to insert lithium ions into the layered structures, followed by exfoliation in water with ultrasonication.[8a,13] However, in addition to the high reaction temperature (e.g. 100 °C) and long reaction time (e.g. 3 days),[8a] another major drawback of this method is the lack of controllability over the degree of lithium insertion. Incomplete lithium intercalation will lead to a low yield of single-layer materials whereas over insertion of lithium can result in decomposition and formation of metal nanoparticles and Li_2S.[14] Recently, through a sulfidation-induced shape transformation process, 2D WS_2 sheets were successfully prepared from 1D $W_{18}O_{49}$ nanorods, but the lateral dimension of the WS_2 sheets was only around 100 nm, which was restricted by the size of the rods.[3b]

Herein, we develop a simple but effective method to fabricate high-yield, single-layer 2D nanomaterials, through a controllable lithiation process. By incorporating the layered bulk materials, such as MoS_2, WS_2, TiS_2, TaS_2, ZrS_2, and graphite, as the cathode in an electrochemical set-up, the lithium intercalation in these materials can be monitored and finely controlled during the discharge process. With subsequent ultrasonication and exfoliation of these intercalated compounds in water or ethanol, high-yield single-layer nanosheets of these materials can be prepared in large amounts for subsequent thin-film and device fabrications.

The electrochemical lithiation process was carried out in a battery test system as illustrated in Figure 1. The layered bulk material, that is, MoS_2, WS_2, TiS_2, TaS_2, ZrS_2 or graphite, was incorporated in a test cell as cathode (Step 1 in Figure 1). The lithium foil was used as anode to provide lithium ions. The lithium intercalation process was conducted at a galvanostatic discharge with a current density of 0.05 mA. After completion of the lithium insertion (Step 2 in Figure 1), the intercalated compound (e.g. Li_xMoS_2) was washed with acetone to remove the residual electrolyte (i.e. $LiPF_6$), and then ultrasonicated in water or ethanol to exfoliate and isolate the 2D nanosheets

[*] Z. Zeng, Dr. Z. Yin,[+] Dr. X. Huang,[+] Dr. H. Li, Q. He, G. Lu, Prof. F. Boey, Prof. H. Zhang
School of Materials Science and Engineering
Nanyang Technological University
50 Nanyang Avenue, Singapore 639798 (Singapore)
E-mail: hzhang@ntu.edu.sg
hzhang166@yahoo.com
Homepage: http://www.ntu.edu.sg/home/hzhang/

[+] These authors contributed equally to this work.

[**] This work was supported by AcRF Tier 2 (ARC 10/10, No. MOE2010-T2-1-060) from MOE and New Initiative Fund FY 2010 (M58120031) from NTU in Singapore.

Supporting information for this article is available on the WWW under http://dx.doi.org/10.1002/anie.201106004.

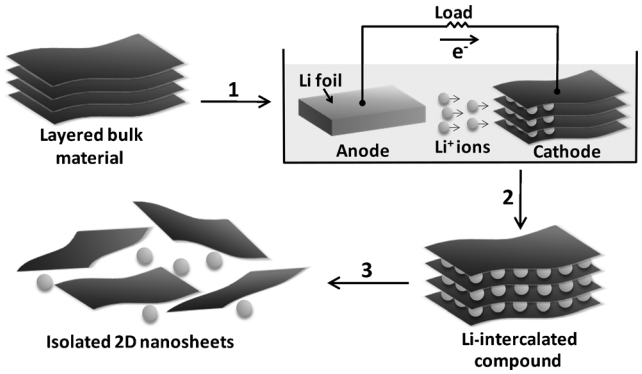

Figure 1. Electrochemical lithiation process for the fabrication of 2D nanosheets from the layered bulk material.

(Step 3 in Figure 1). Here, lithium plays dual roles. First, with the insertion of Li^+ ions into the interlayer spaces of the bulk materials, the interlayer distance is expanded, which weakens the van der Waals interactions between the layers. Second, metallic Li (after insertion Li^+ ions are reduced by electrons during the discharge process) reacts with water to form Li(OH) and H_2 gas (evidently, bubbles were observed during our experiments),[13b,15] which pushes the layers further apart. After providing sufficient agitation by ultrasonication, isolated 2D nanosheets can be obtained. The resulting solution was then centrifuged and washed with water six times and redispersed in water (inset of Figure 2a). The quantity of

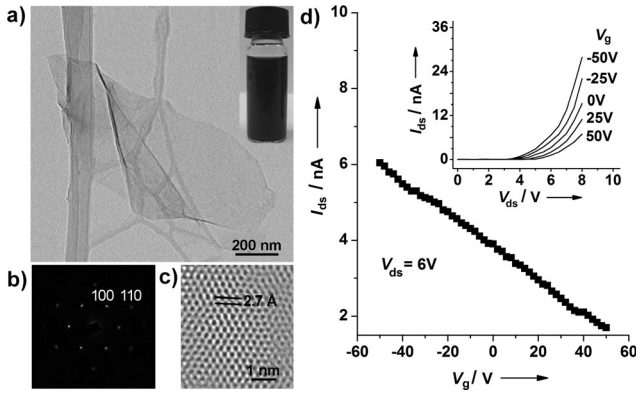

Figure 2. a) TEM image of a typical MoS_2 nanosheet. Inset: Photograph of the MoS_2 solution. b) Selected area electron diffraction (SAED) pattern of a single-layer MoS_2 nanosheet. c) HRTEM image of single-layer MoS_2 nanosheet. d) Plot of the drain-to-source current (I_{ds}) versus the gate voltage (V_g) at a drain voltage (V_{ds}) of 6 V. Inset: Plot of the drain-to-source current versus the drain voltage.

produced nanosheets using our method depends on the effective area of the electrode, which is coated by a slurry of the bulk precursor. For example, in our experiments, we used a copper electrode of a 1.1 cm^2 area to prepare around 2 mg of nanosheets. Further scale-up production of nanosheets can be realized by increasing the size of the electrode.

The chemical composition of the obtained nanosheets was studied by energy dispersive X-ray spectroscopy (EDS) and X-ray photoelectron spectroscopy (XPS). EDS analysis reveals that the obtained nanosheets are comprised of stoichiometric MoS_2 (see Figure S1 in Supporting Information), and XPS spectra show strong $Mo3d_{5/2}$ and $S2p_{3/2}$ bands at 229.8 and 162.7 eV, respectively, indicating that Mo^{4+} and S^{2-} are the dominant oxidation states (see Figure S2 in the Supporting Information).[16] Figure 2a shows the transmission electron microscopy (TEM) image of a typical MoS_2 nanosheet. The electron diffraction pattern of a flat area of the nanosheet (Figure 2b) and the corresponding high-resolution TEM (HRTEM) image (Figure 2c) show the hexagonal lattice structure with a lattice spacing of 2.7 Å assigned to the (100) planes.[17] The atomic force microscopy (AFM) measurement of a typical MoS_2 sheet reveals a thickness of around 1.0 nm (see Figure S3a in the Supporting Information), which confirms a single-layer MoS_2 nanosheet. In addition, the preparation of large amounts of single-layer MoS_2 nanosheets by our method was monitored by AFM measurements of 100 MoS_2 nanosheets, which showed that 92% of the sheets are single-layered (see Figure S3b–e in the Supporting Information). This high-yield production of single-layer MoS_2 nanosheets was further confirmed by X-ray diffraction (XRD) analysis (see Figure S4 in the Supporting Information). Based on the previous theoretical calculation[13b] and experimental study,[8a] the absence of a peak (002) at around 14.5° (see Figure S4b in the Supporting Information), which belongs to the bulk MoS_2 (see Figure S4a in the Supporting Information), suggests the successful fabrication of large-amount single-layer MoS_2 nanosheets. The peaks associated with the MoS_2 planes that are not parallel to the basal plane of the nanosheet are not observed because the nanosheets mostly lie on the glass substrate.

The electronic structure of the obtained MoS_2 nanosheets was examined by Raman spectroscopy (see Figure S5 in the Supporting Information). A typical single-layer MoS_2 nanosheet (confirmed by AFM) gives bands at 382.1 and 407.5 cm^{-1}, which are associated to the E^1_{2g} and A_{1g} modes[18] with full widths at half maximum (FWHM) of 18.4 and 16.0 cm^{-1}, respectively. The corresponding bands for bulk MoS_2 are located at 380.7 and 406.2 cm^{-1} with FWHM of 6.6 and 7.3 cm^{-1}, respectively. The single-layer MoS_2 nanosheet exhibits much broader bands relative to the bulk counterpart, which is due to the phonon confinement in the ultra-thin structure.[8a]

In addition, under laser excitation at 488 nm, the room temperature photoluminescence (PL) spectrum of a single-layer MoS_2 nanosheet (see Figure S6 in the Supporting Information) exhibits a peak centered at 667 nm (1.86 eV) with an FWHM of 33 meV and a shoulder at 618 nm (2.01 eV), which is consistent with mechanically cleaved single-layer MoS_2.[19] The peak at 667 nm is attributed to the direct electron–hole transition that leads to the high relaxation rate for intraband carriers towards the conduction/valence band minimum, whereas the relatively weak shoulder (618 nm) originates from the spin–orbital splitting of the valence band energy.[19b]

Importantly, our facile method for large-amount, high-yield production of single-layer nanosheets and solution-phase processability provides a broad range of applications. As a proof of concept, a single-layer MoS_2-based field-effect

transistor (FET; see Figure S7 in the Supporting Information) was fabricated by drop-casting the aqueous MoS_2 nanosheet solution onto a Si/SiO_2 substrate, followed by fabrication of Ti/Au electrodes on a single-layer MoS_2 with e-beam lithography. The recorded *I–V* characteristic curve at vacuum (around 10^{-5} Torr) indicates *p*-type doping of the single-layer MoS_2 (Figure 2d), which is different from *n*-type doping of the MoS_2 exfoliated by scotch tape[3d,20] or sonication.[11] This difference might arise from the fact that electrons were transferred from the residual lithium to MoS_2, resulting in a more than half-filled band in MoS_2 and consequently leading to *p*-type doping of the obtained single-layer MoS_2 nanosheet.[21]

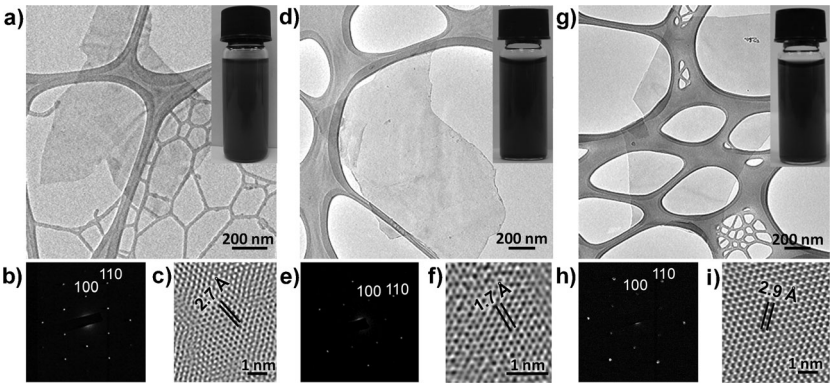

Figure 3. a) TEM image of a typical single-layer WS_2 nanosheet. Inset: Photograph of the WS_2 solution. b) SAED pattern of a single-layer WS_2 nanosheet. c) HRTEM image of a single-layer WS_2 nanosheet. d) TEM image of a typical single-layer TiS_2 nanosheet. Inset: Photograph of a TiS_2 solution. e) SAED pattern of a single-layer TiS_2 nanosheet. f) HRTEM image of a single-layer TiS_2 nanosheet. g) TEM image of a typical single-layer TaS_2 nanosheet. Inset: Photograph of the TaS_2 solution. h) SAED pattern of a single-layer TaS_2 nanosheet. i) HRTEM image of single-layer TaS_2 nanosheet.

To further demonstrate the advantage of our method for high-yield preparation of single-layer nanosheets, the obtained MoS_2 nanosheets were used to fabricate thin-film transistors (TFTs). The spin-coated MoS_2 thin film was electrically conductive over large areas (see Figure S8 in the Supporting Information). After Au electrodes were deposited by thermal evaporation, the resulting MoS_2 TFT was used to detect the adsorption of NO. The current response of the MoS_2 film gas sensor towards a different concentration of NO (from 0.4 to 5 ppm) is shown in Figure S9A in the Supporting Information. The adsorption of NO molecules caused an increase in the current at a continuous NO flow, whereas the desorption of NO molecules caused a decrease in conductance under conditions in pure N_2 flow. Because of the *p*-type MoS_2 channel, the increase of conductance upon exposure to NO can be attributed to the *p*-type doping effect of the electron-withdrawing NO molecules.[22] Figure S9B in the Supporting Information shows a plot of the current change versus the concentration of NO gas. The detection limit of our gas sensor was calculated to be 190 ppt when ΔI is three times the standard deviation of I_0 (i.e. signal-to-noise ratio = 3), which is lower than the detection limit obtained in graphene-based TFTs,[22–23] suggesting that our MoS_2 TFT provided a promising sensing platform.

Besides MoS_2, our method has also been applied to prepare other single-layer semiconducting nanosheets, such as WS_2, TiS_2, TaS_2, ZrS_2, and graphene. The obtained WS_2 nanosheets were characterized and the results are shown in Figure 3a–c. Similar to MoS_2, the WS_2 nanosheet shows the hexagonal lattice structure (Figure 3b), with a lattice spacing of 2.7 Å measured by HRTEM (Figure 3c), which is consistent with the spacing of the WS_2 (100) planes.[8a,24] AFM measurements on a typical WS_2 nanosheet reveal an average thickness of around 1.0 nm (see Figure S10 in the Supporting Information), which confirms the successful fabrication of single-layer WS_2 nanosheets (the interlayer distance of WS_2 is around 0.6 nm[3b,24]).

TEM analyses of the obtained TiS_2 and TaS_2 nanosheets are shown in Figure 3d–f and Figure 3g–i, respectively. The crystal structures of TiS_2 and TaS_2 studied here belong to the trigonal system (space group $P\bar{3}1c$),[25] which is different from the hexagonal structure (space group $P63/mmc$) of MoS_2 and WS_2.[26] This difference is shown by the selected area electron diffraction (SAED) patterns of TiS_2 (Figure 3e) and TaS_2 (Figure 3h), that is, the outer six spots of the (110) planes are brighter than the inner ones of the (100) planes, which is different from the patterns observed for single-layer MoS_2 (Figure 2b) and WS_2 nanosheets (Figure 3b). The measured lattice spacing of 1.7 Å for the (110) planes in TiS_2 (Figure 3f) and 2.9 Å for the (100) planes in TaS_2 (Figure 3i) are consistent with the respective theoretical values.[25] The thickness of typical TiS_2 and TaS_2 nanosheets measured by AFM is around 0.7 and 1.0 nm, respectively (see Figures S11 and S12 in the Supporting Information), confirming the production of single-layer nanosheets. In addition, the single-layer ZrS_2 and graphene nanosheets have also been successfully produced by our method (the results are shown in Figures S13 and S14 in the Supporting Information).

Compared to the traditional lithium intercalation method, which uses the expensive *n*-butyllithium as the intercalate, requires elevated reaction temperatures (e.g. 100 °C) and takes three days,[8a] our electrochemical lithiation method can be easily conducted at room temperature within 6 h. More importantly, the lithiation process can be monitored and finely controlled in the battery test system. For example, the lithiation process of MoS_2 was monitored by a galvanostatic discharge curve (discharge voltage versus lithium content *x*, as in Li_xMoS_2). As shown in Figure S15 in the Supporting Information, the cell voltage decreases rapidly from 1.8 to 1.2 V in the range of $0 < x < 0.2$, and at $x \approx 0.2$, a plateau occurs which lasts till $x \approx 1.3$, indicating a phase transition of the compound. As reported previously, the lithium insertion of MoS_2 was considered to involve a two-phase transition process, from trigonal prismatic (2H) to octahedral (1T) coordination.[26,27] At about $x = 1.3$, the 2H to 1T phase transformation is completed. During the phase transformation, lithium atoms reside in the octahedral and tetrahedral interstices of the MoS_2 layers, enlarging the distance between

the layers bound by van der Waals forces.[26] However, the over insertion of Li resulted in the decomposition of MoS_2 and formation of Mo nanoparticles and Li_2S.[27a] Indeed, Mo nanoparticles were observed on the MoS_2 nanosheets (see Figure S16 in the Supporting Information), when the reaction was carried at a lithium content x of about 3. Therefore, this in situ monitoring allows us to stop the reaction at a proper Li content to avoid the decomposition of intercalated compounds.

In summary, we have developed a simple but effective approach to fabricate high-yield, single-layer semiconducting nanosheets, based on a controllable electrochemical lithiation process. By incorporating the layered bulk materials, such as MoS_2, WS_2, TiS_2, TaS_2, ZrS_2 or graphite, as cathode in an electrochemical cell, the lithium intercalation in the bulk material can be monitored and finely controlled during the discharge process. After subsequent ultrasonication and exfoliation of these intercalated compounds in water or ethanol, high-yield, single-layer nanosheets can be prepared in large amounts. In particular, the large-scale production of single-layer MoS_2 has been achieved in 92% yield. As a proof of concept, a single-layer MoS_2-based FET device is fabricated, showing its *p*-type semiconducting property. The TFT based on MoS_2 films was also prepared for detection of NO. In conclusion, we provide a novel, facile, fast, and highly controllable method for the synthesis of large-amount, high-yield, single-layer 2D semiconducting nanosheets (analogous to graphene), which can be used for various applications in electric devices, heterogeneous catalysis, and gas sensors.

Experimental Section

Chemicals: Molybdenum disulfide (MoS_2; 10–30 μm, Rose Mill, West Hartford, USA), tungsten (IV) disulfide (WS_2, Sigma, Steinheim, Germany), titanium (IV) sulfide (TiS_2, Sigma, Steinheim, Germany), tantalum (IV) sulfide (TaS_2, Alfa Aeser, Massachusetts, USA), zirconium (IV) sulfide (ZrS_2, Strem, Massachusetts, USA), natural graphite (Bay carbon Inc, Michigan, USA), poly(vinylidene fluoride) (PVDF, Sigma, Steinheim, Germany), *N*-methylpyrrolidone (Sigma, Steinheim, Germany), 3-aminopropyltriethoxysilane (APTES, Sigma, Steinheim, Germany), the lithium ion battery electrolyte (Charslton Technologies Pte Ltd., International Business Park, Singapore), the lithium foil (ACME Research Support Pte Ltd, Bukit Batok Street, Singapore), the polypropylene (pp) film (Celgard 2300, North Carolina, USA), the copper foil (ACME Research Support Pte Ltd, Bukit Batok Street, Singapore), acetone (Tech Grade, Aik Moh Paints & Chemicals Pte Ltd, Singapore), and ethanol (>99.9%, Merck, Darmstadt, Germany) were used as received without further purification. The deionized water was purified using Milli-Q System (Millipore, Billerica, MA, USA).

Electrochemical intercalation: The lithium intercalation of the layered materials was performed in a test cell using the Li foil as anode and 1M $LiPF_6$ as electrolyte, which was dissolved in a mixture of ethyl carbonate (EC) and dimethyl carbonate (DMC) at a volume ratio of 1:1. The layered bulk material (i.e. MoS_2, WS_2, TiS_2, TaS_2, ZrS_2 or graphite) was prepared as cathode by mixing with acetylene black and poly(vinylidene fluoride) (PVDF) binder dispersed in *N*-methylpyrrolidone (NMP) solutions. In the mixed slurry, the mass ratio of the layered bulk material, acetylene black, and PVDF was 80:10:10. The resulting slurry was then uniformly coated on a copper foil and dried under vacuum overnight. The assembly of the test cells for different layered materials was conducted in an Ar-filled glove box. The electrochemical intercalation of the layered materials in the test cell was accomplished in a Neware battery test system at room temperature. The electrochemical intercalation was performed using galvanostatic discharge at current density of 0.05 mA. After the discharge process, the Li-intercalated sample was washed with acetone to remove any residual electrolyte ($LiPF_6$), followed by exfoliation and ultrasonication in distilled water or ethanol in a closed vial, during which the profuse evolution of gas was observed and an opaque suspension of the layered materials formed. After the suspension was centrifuged and washed six times with water, it was collected for further characterizations.

Fabrication of a single-layer MoS_2 field-effect transistor (FET): An aqueous solution of suspended MoS_2 nanosheets (0.1 $mg\,mL^{-1}$) was drop-cast onto the O_2 plasma-cleaned Si/SiO_2 (200 nm) substrate, followed by annealing at 450°C for 2 h in Ar. Then Ti (10 nm)/Au (50 nm) electrodes were fabricated by e-beam lithography (EBL), which were covered on a single-layer MoS_2 nanosheet (see Figure S7 in the Supporting Information). The current–voltage (I-V) curve of the obtained device was tested in a vacuum chamber at around 10^{-5} Torr to avoid any doping effect induced by air.

Fabrication of MoS_2 thin-film transistors (TFTs) for sensing of NO: The aqueous solution of MoS_2 was centrifuged at 8000 rpm and re-dispersed in methanol with ultrasonication. The stable methanol solution of MoS_2 was then spin-coated on a Si/SiO_2 substrate at 4000 rpm. The thickness of the MoS_2 film was controlled by the volume of the MoS_2 solution used during the spin-coating process. The as-prepared MoS_2 thin film was further dried under vacuum at room temperature for 2 h before it was used for fabrication of a thin-film transistor. Au (50 nm) was deposited as drain and source electrodes by thermal evaporation. The width and length of the MoS_2 channel were 400 μm and 5 mm, respectively. The gas sensing was carried out in a continuous flow of NO gas (at a certain concentration of N_2) on the MoS_2 surface by monitoring the drain to source current continuously. The desorption process was carried out by switching the NO flow to pure N_2 flow. The concentration of NO was controlled by the flow ratio of NO (5 ppm) and N_2. All experiments were performed in air at room temperature.

Characterization: A drop of a solution containing the produced 2D nanomaterials was placed on a holey carbon-coated copper grid, APTES-modified Si/SiO_2, Si/SiO_2, APTES-modified Si/SiO_2, Si/SiO_2, and glass, and then dried in air prior to its characterization by transmission electron microscopy (TEM, JEM 2100F), scanning electron microscopy (SEM, JSM-7600) coupled with energy dispersive X-ray spectroscopy (EDS), X-ray photoelectron spectroscopy (XPS, Axis Ultra), atomic force microscopy (AFM, Dimension 3100, Veeco, CA), Raman spectroscopy (WITec alpha 300 confocal Raman microscope), and X-ray diffraction (XRD, Shimadzu), respectively. For photoluminescence (PL) studies, single-layer MoS_2 nanosheet was deposited on a APTES-modified Si/SiO_2 substrate (confirmed by AFM), followed by annealing at 450°C for 2 h in Ar. The PL spectrum was measured in air at room temperature by using laser light of 488 nm as the source of excitation.

Received: August 25, 2011
Revised: September 24, 2011
Published online: October 21, 2011

Keywords: electrochemistry · nanomaterials · nanosheets · semiconductors · sensors

[1] a) M. Osada, T. Sasaki, *J. Mater. Chem.* **2009**, *19*, 2503–2511; b) C. Wang, Y. Zhou, M. Ge, X. Xu, Z. Zhang, J. Z. Jiang, *J. Am. Chem. Soc.* **2009**, *132*, 46–47; c) T. Yu, B. Lim, Y. Xia, *Angew. Chem.* **2010**, *122*, 4586–4589; *Angew. Chem. Int. Ed.* **2010**, *49*, 4484–4487.

[2] a) A. K. Geim, *Science* **2009**, *324*, 1530–1534; b) X. Huang, X. Y. Qi, F. Boey, H. Zhang, *Chem. Soc. Rev.* **2012**, DOI:

10.1039/C1031CS15078B; c) X. Huang, Z. Yin, S. Wu, X. Qi, Q. He, Q. Zhang, Q. Yan, F. Boey, H. Zhang, *Small* **2011**, *7*, 1876 – 1902.

[3] a) R. R. Chianelli, M. H. Siadati, M. P. De La Rosa, G. Berhault, J. P. Wilcoxon, R. Bearden, B. L. Abrams, *Catal. Rev. Sci. Eng.* **2006**, *48*, 1 – 41; b) J. W. Seo, Y. W. Jun, S. W. Park, H. Nah, T. Moon, B. Park, J. G. Kim, Y. J. Kim, J. Cheon, *Angew. Chem.* **2007**, *119*, 8984 – 8987; *Angew. Chem. Int. Ed.* **2007**, *46*, 8828 – 8831; c) A. Ayari, E. Cobas, O. Ogundadegbe, M. S. Fuhrer, *J. Appl. Phys.* **2007**, *101*, 014507; d) H. Li, Z. Y. Yin, Q. Y. He, H. Li, X. Huang, G. Lu, D. W. H. Fam, A. I. Y. Tok, Q. Zhang, H. Zhang, *Small* **2011**, DOI: 10.1002/smll.201101016.

[4] A. Nag, K. Raidongia, K. P. S. S. Hembram, R. Datta, U. V. Waghmare, C. N. R. Rao, *ACS Nano* **2010**, *4*, 1539 – 1544.

[5] K. S. Novoselov, D. Jiang, F. Schedin, T. J. Booth, V. V. Khotkevich, S. V. Morozov, A. K. Geim, *Proc. Natl. Acad. Sci. USA* **2005**, *102*, 10451 – 10453.

[6] L. Y. Jiao, L. Zhang, X. R. Wang, G. Diankov, H. J. Dai, *Nature* **2009**, *458*, 877 – 880.

[7] H. Zeng, C. Zhi, Z. Zhang, X. Wei, X. Wang, W. Guo, Y. Bando, D. Golberg, *Nano Lett.* **2010**, *10*, 5049 – 5055.

[8] a) H. S. S. Ramakrishna Matte, A. Gomathi, A. K. Manna, D. J. Late, R. Datta, S. K. Pati, C. N. R. Rao, *Angew. Chem.* **2010**, *122*, 4153 – 4156; *Angew. Chem. Int. Ed.* **2010**, *49*, 4059 – 4062; b) Y. Shi, C. Hamsen, X. Jia, K. K. Kim, A. Reina, M. Hofmann, A. L. Hsu, K. Zhang, H. Li, Z.-Y. Juang, M. S. Dresselhaus, L.-J. Li, J. Kong, *Nano Lett.* **2010**, *10*, 4134 – 4139; c) L. Song, L. Ci, H. Lu, P. B. Sorokin, C. Jin, J. Ni, A. G. Kvashnin, D. G. Kvashnin, J. Lou, B. I. Yakobson, *Nano Lett.* **2010**, *10*, 3209 – 3215.

[9] Y. Hernandez, V. Nicolosi, M. Lotya, F. M. Blighe, Z. Sun, S. De, I. T. McGovern, B. Holland, M. Byrne, Y. K. Gun′Ko, J. J. Boland, P. Niraj, G. Duesberg, S. Krishnamurthy, R. Goodhue, J. Hutchison, V. Scardaci, A. C. Ferrari, J. N. Coleman, *Nat. Nanotechnol.* **2008**, *3*, 563 – 568.

[10] C. Y. Zhi, Y. Bando, C. C. Tang, H. Kuwahara, D. Golberg, *Adv. Mater.* **2009**, *21*, 2889 – 2893.

[11] J. N. Coleman, M. Lotya, A. O'Neill, S. D. Bergin, P. J. King, U. Khan, K. Young, A. Gaucher, S. De, R. J. Smith, I. V. Shvets, S. K. Arora, G. Stanton, H.-Y. Kim, K. Lee, G. T. Kim, G. S. Duesberg, T. Hallam, J. J. Boland, J. J. Wang, J. F. Donegan, J. C. Grunlan, G. Moriarty, A. Shmeliov, R. J. Nicholls, J. M. Perkins, E. M. Grieveson, K. Theuwissen, D. W. McComb, P. D. Nellist, V. Nicolosi, *Science* **2011**, *331*, 568 – 571.

[12] M. B. Dines, *J. Chem. Educ.* **1974**, *51*, 221 – 223.

[13] a) M. B. Dines, *Mater. Res. Bull.* **1975**, *10*, 287 – 291; b) P. Joensen, R. F. Frindt, S. R. Morrison, *Mater. Res. Bull.* **1986**, *21*, 457 – 461; c) B. K. Miremadi, S. R. Morrison, *J. Appl. Phys.* **1988**, *63*, 4970 – 4974.

[14] X. Rocquefelte, F. Boucher, P. Gressier, G. Ouvrard, *Phys. Rev. B* **2000**, *62*, 2397.

[15] B. K. Miremadi, S. R. Morrison, *J. Catal.* **1991**, *131*, 127 – 132.

[16] M. A. Baker, R. Gilmore, C. Lenardi, W. Gissler, *Appl. Surf. Sci.* **1999**, *150*, 255 – 262.

[17] X. R. Qin, D. Yang, R. F. Frindt, J. C. Irwin, *Ultramicroscopy* **1992**, *42 – 44*, 630 – 636.

[18] S. Jiménez Sandoval, D. Yang, R. F. Frindt, J. C. Irwin, *Phys. Rev. B* **1991**, *44*, 3955.

[19] a) K. F. Mak, C. Lee, J. Hone, J. Shan, T. F. Heinz, *Phys. Rev. Lett.* **2010**, *105*, 136805; b) A. Splendiani, L. Sun, Y. Zhang, T. Li, J. Kim, C.-Y. Chim, G. Galli, F. Wang, *Nano Lett.* **2010**, *10*, 1271 – 1275.

[20] B. Radisavljevic, A. Radenovic, J. Brivio, V. Giacometti, A. Kis, *Nat. Nanotechnol.* **2011**, *6*, 147 – 150.

[21] a) J. Heising, M. G. Kanatzidis, *J. Am. Chem. Soc.* **1999**, *121*, 11720 – 11732; b) R. B. Somoano, V. Hadek, A. Rembaum, *J. Chem. Phys.* **1973**, *58*, 697 – 701.

[22] J. D. Fowler, M. J. Allen, V. C. Tung, Y. Yang, R. B. Kaner, B. H. Weiller, *ACS Nano* **2009**, *3*, 301 – 306.

[23] V. Dua, S. P. Surwade, S. Ammu, S. R. Agnihotra, S. Jain, K. E. Roberts, S. Park, R. S. Ruoff, S. K. Manohar, *Angew. Chem.* **2010**, *122*, 2200 – 2203; *Angew. Chem. Int. Ed.* **2010**, *49*, 2154 – 2157.

[24] W. J. Schutte, J. L. De Boer, F. Jellinek, *J. Solid State Chem.* **1987**, *70*, 207 – 209.

[25] a) C. Riekel, R. Schöllhorn, *Mater. Res. Bull.* **1975**, *10*, 629 – 633; b) M. Bovet, S. van Smaalen, H. Berger, R. Gaal, L. Forró, L. Schlapbach, P. Aebi, *Phys. Rev. B* **2003**, *67*, 125105.

[26] K. Chrissafis, M. Zamani, K. Kambas, J. Stoemenos, N. A. Economou, I. Samaras, C. Julien, *Mater. Sci. Eng. B* **1989**, *3*, 145 – 151.

[27] a) L. S. Selwyn, W. R. McKinnon, U. von Sacken, C. A. Jones, *Solid State Ionics* **1987**, *22*, 337 – 344; b) C. M. Julien, *Mater. Sci. Eng. R* **2003**, *40*, 47 – 102.

